Journal of Geoscience and Environment Protection, 2026, 14(2), 157-175
https://www.scirp.org/journal/gep
ISSN Online: 2327-4344
ISSN Print: 2327-4336

A Multi-Metric and Multi-Driver Analysis of Long-Term Aridity Change over Africa (1951-2020)

Noel Banda[1,2*], Tanimu Abubakar Sadiq[1,3], Tianyu Wang[4], Nyasulu Matthews[5]

[1]School of Atmospheric Science, Nanjing University of Information Science and Technology (NUIST), Nanjing, China
[2]Department of Climate Change and Meteorological Services (DCCMS), Blantyre, Malawi
[3]Nigerian Meteorological Agency (NiMet), Nnamdi Azikiwe International Airport, Abuja, Nigeria
[4]State Key Laboratory of Climate System Prediction and Risk Management/Key Laboratory of Meteorological Disaster, Ministry of Education/Collaborative Innovation Center on Forecast and Evaluation of Meteorological Disasters/Institute for Climate and Application Research/Jiangsu Key Laboratory of Intelligent Weather Forecasting and Applications Based on Big Data, Nanjing University of Information Science and Technology, Nanjing, China
[5]School of Ecology and Applied Meteorology, Nanjing University of Information Science and Technology (NUIST), Nanjing, China
Email: *bandanoxy@gmail.com

How to cite this paper: Banda, N., Sadiq, T. A., Wang, T. Y., & Matthews, N. (2026). A Multi-Metric and Multi-Driver Analysis of Long-Term Aridity Change over Africa (1951-2020). *Journal of Geoscience and Environment Protection, 14,* 157-175.
https://doi.org/10.4236/gep.2026.142009

Received: January 15, 2026
Accepted: February 10, 2026
Published: February 13, 2026

Abstract

Africa is highly vulnerable to growing aridification, with more than 60% of the total area classified as arid, supporting more than half a billion people (~525 million). Despite widespread drying, the climatic drivers of the long-term dryness remain uncertain. We employed a multi-metric framework to assess the climatic components of growing aridification in Africa using the Aridity Index (AI) and its climatic drivers, precipitation (P) and potential evapotranspiration (PET), during 1951-2020. Our results suggest widespread drying trends across 88.9% of Africa, with nearly half of it, about 43%, experiencing significant dryness. We reveal that increasing PET in about 85.7% of the continent emerges as a dominant driver of drying, compared to precipitation-driven drying, which covers roughly 20.3%, suggesting that atmospheric moisture demand might play a leading role. Further analysis of PET decomposition indicates that warming temperatures are the main driver of rising atmospheric moisture demand, in line with anthropogenic global climate warming. This trend is evident in accelerated dryland expansion since 1985, particularly over southern, eastern, and western Africa, where drylands are rapidly expanding. Net drying dominates most regions. East Africa, in contrast, exhibits a more complex pattern characterized by seasonal moistening, reflecting complex hydroclimatic responses. These results demonstrate that increasing PET induced by warming

is the main contributor to increasing dryness in Africa, while precipitation changes play a secondary role. We propose that adaptation strategies consider both the rising atmospheric moisture demand and rainfall variability under continued global climate warming.

Keywords

Aridification, Aridity Index, Potential Evapotranspiration, Climate Change, Africa

1. Introduction

In recent decades, most parts of the world have been facing growing aridity as these areas are transitioning into arid conditions (Sardans et al., 2024). Water scarcity and land degradation are some of the evidence of growing aridity which have been observed across North America, Brazil, Europe, Africa, the Middle East, Central Asia, and Australia (Feng & Fu, 2013). This means areas which were already arid continue to suffer. In dryland regions, more than half of global drylands account for most of the aridity expansion with varying intensity (Huang et al., 2016). Therefore, understanding aridity change is essential for Africa, whose land is approximately 60% classified as dryland and over half a billion people (~525 million) are living here and survive by farming activities in these areas (De Haan, 2016; Li et al., 2024).

Aridity is defined as the measure of dryness occurring over an extended period of time, and these conditions reflect long-term water unavailability, determined by the balance between precipitation and potential evapotranspiration (Greve et al., 2017, 2019). Findings from previous studies show that precipitation alone underestimates drying trends, meaning that considering other parameters in assessing aridity is crucial. As global temperatures continue to rise, this has an effect on potential evapotranspiration, possibly intensifying aridification (Lim Kam Sian et al., 2024). Studies have suggested the use of multiple approaches that integrate precipitation, potential evapotranspiration, and other hydroclimatic drivers for a better understanding of aridity dynamics (Liu & Zhou, 2023; Ullah et al., 2022).

Early research attempted to link rainfall and aridity patterns in Africa to the movement of regional and global large-scale climate systems. Mohino et al. (2024) observed that a positive phase of Atlantic Multidecadal Variability (AMV) led to extreme weather events and a lot of rainfall in the Sahel region. In contrast, observations in East and Southern Africa indicate that alternating wet and dry years are suggested to be driven by the combined effect of the El Niño–Southern Oscillation (ENSO), which interacts with the Indian Ocean Dipole (IOD) to influence rainy weather in the region (Cai et al., 2025). The weakening of large-scale teleconnections across Africa since the 1970s to 1980s was linked to changes in ENSO-related influences and equatorial atmospheric circulation (Nicholson et al., 2018). Together, these studies highlight the importance of large-scale climate driv-

ers and regional variability when assessing African drylands.

The majority of Africa is not spared from the impacts of growing aridity. These impacts include recurring drought events, reduced agricultural yield, and soil degradation, which are results of dryland expansion across the Sahara, Sahel, East, and Southern Africa (Akpa, 2024; Ayugi et al., 2022; Bedair et al., 2023; Masih et al., 2014). Sahel, Horn of Africa, and Southern Africa suffer from drought events, which lead to yield reductions for crops like maize, rice, and sorghum (Akpa, 2024). Climate extremes affect agriculture and water resources in sub-Saharan Africa, implying that long-term dryness affects most aspects of life (Abate et al., 2025). In addition, societies cope with growing aridity differently, for example in the Sahelian drylands, where ecosystems respond differently to drought and land degradation (Dendoncker et al., 2023). In the West African savanna region, farmers show resilience by practicing climate-smart farming, empowering women, and generating off-farm income (Yessoufou et al., 2024). In northern and Southern Africa, the case is different, as these areas were identified as aridification hotspots, meaning disturbance in the climate results in overwhelming impacts. Among them, the ongoing global warming is therefore expected to intensify dry conditions and worsen the risks to water availability, land, and livelihoods (Feng & Fu, 2013). It is vital to formulate and implement adaptation strategies that are centered on supporting dryland management, conservation agriculture, and community-based adaptation practices to enhance resilience (Li et al., 2024; Wei et al., 2021). Knowledge gaps still exist despite efforts made in most studies on aridification, since they rarely relate precipitation decline and potential evapotranspiration increases to aridity in Africa. A number of studies at the regional level provided some insights; for instance, in West Africa, rising temperatures and PET over the past four decades drove significant aridity and dryland expansion (Daramola et al., 2023). Studies conducted over East Africa show that temperature-driven evaporative demand possibly causes aridity based on past three decades of observations (Ayugi et al., 2025). Generally, these studies show the importance of including more factors to assess aridity rather than traditional rainfall pattern analysis. In our research, we attempt to address these gaps by using a multi-metric and multi-driver approach to study aridity over Africa between 1951 and 2020. In our approach, we try to quantify the magnitude and spatial extent of changes in dryness and then attribute these changes to potential evapotranspiration and its components. Lastly, we assess whether these patterns are shifting and expanding across Africa. This approach contributes relevant knowledge on how and why Africa's drylands are changing and suggests possible adaptation strategies.

2. Study Area, Datasets, and Methods

2.1. Study Area

The African continent, covering latitude 35˚00'S to 52˚00'N and longitudes from 24˚00'W to 32˚00'E, was subdivided into nine sub-regions in the recent Intergovernmental Panel on Climate Change Sixth Assessment Report (IPCC AR6) (Iturbide et

al., 2020). Some studies considered three divisions for Africa (Qiao et al., 2022). In this study, four domains were used based on hydroclimatic zones, namely, North Africa (15.5˚N-37.5˚N, 18˚W-37.5˚E), West Africa (11.5˚S-15˚N, 18˚W–30˚E), East Africa (11.5˚S-15˚N, 30.5˚-52˚E), and Southern Africa (35˚-12˚S, 11˚-52˚E), as illustrated in **Figure 1(a)**. These divisions enable us to detect how each region responds to climate conditions without generalizing continent patterns. North Africa comprises the hyper-arid Sahara Desert, regarded as a climate change hotspot characterized by high temperatures, water scarcity, and frequent drought (Schilling et al., 2020). West Africa, as defined in this study to include the Central African domain, is dominated by the West African Monsoon and the influence of the Congo Rainforest Basin, driving a north to south rainfall gradient and high annual rainfall over the equatorial region (Nicholson, 2013). Rainfall in the southern and equatorial parts of the region is influenced by strong local moisture recycling and large-scale circulation patterns, driving moisture from the Atlantic and Indian Oceans (Dyer et al., 2017). East Africa has a bimodal rainfall pattern, from March to May, known as the "long rain" period, and October to December "short rain", which is becoming wetter. Approximately 75% of the land is classified as arid to semi-arid, impacting various sectors (Ayugi et al., 2025). In addition to West Africa, the Southern African climate is largely controlled by the oscillation of the Intertropical Convergence Zone (ITCZ) and ENSO variability, with El Niño typically inducing drought conditions (Cai et al., 2025). This regional division provides the essential spatial context for analyzing the drivers and impacts of aridity changes across the continent's diverse climates.

2.2. Datasets

The study employed precipitation data obtained from the Global Precipitation Climatology Centre (GPCC) full data Monthly Version 2023 (Schneider et al., 2022), providing a gridded dataset at a resolution of 0.25˚ × 0.25˚ covering the entire African continent for the study period from 1951 to 2020. Potential evapotranspiration (PET) was computed from surface net radiation (R_n), relative humidity (RH), and wind speed (U), which we obtained from the ERA5-Land reanalysis dataset available at 0.1˚ × 0.1˚ resolution (Muñoz-Sabater et al., 2021). The precipitation was regridded from 0.25˚ × 0.25˚ resolution to match the ERA5-Land grid using linear interpolation for aridity index calculations. This approach of regridding data to a common grid minimizes scale mismatches when working with data from different sources, types, or resolutions. Several studies in climate science research use this practice; for example, temperature and multiple precipitation were regridded to get a common grid for trend analysis and other statistics in Hassler & Lauer (2021). Similarly, Noël et al. (2022) used the ERA5-Land reanalysis dataset as a reference while downscaling and regridding precipitation and temperature datasets to obtain higher resolution data from 0.25˚ × 0.25˚ to 0.1˚ × 0.1˚. These datasets were collectively used to assess aridity trends, spatial distribution, and corresponding contributions for annual and seasonal time scales. The

data were aggregated from monthly values to standard seasons (DJF, MAM, JJA, SON) and annual means for further trend analysis across space and time.

2.3. Methods

The AI was used in this study as a standardized measure of dryness, and was defined as the ratio of precipitation to PET, representing water supply and atmospheric water demand, respectively:

$$\mathrm{AI} = \frac{\mathrm{P}}{\mathrm{PET}} \tag{1}$$

In Equation (1), P is the total precipitation (mm) and PET is the potential evapotranspiration (mm). The AI classification follows the United Nations Environment Programme (UNEP) scheme (Middleton & Thomas, 1997) and is divided into Hyper-arid (AI < 0.05), Arid (0.05 ≤ AI < 0.20), Semi-arid (0.20 ≤ AI < 0.50), Dry subhumid (0.50 ≤ AI < 0.65), and Humid (AI ≥ 0.65) (Middleton & Thomas, 1997; Mortimore & Anderson, 2009). This categorization has been extensively adopted in many studies (Daramola et al., 2023; Feng & Fu, 2013; Liu & Zhou, 2023; Scheff & Frierson, 2015).

PET was estimated using the FAO Penman-Monteith method shown in Equation (2), a standardized method for reference evapotranspiration by Allen et al. (1998). Monthly gridded datasets were used for the required meteorological variables in this calculation as follows: T, R_n, RH, and U, as shown in the general form of Equation (2) below.

$$PET = \frac{0.408\Delta\left(R_n - G\right) + \gamma \dfrac{(900)}{(T+273)} U_2 \left(e_s + e_a\right)}{\Delta + \gamma\left(1 + 0.34U_2\right)} \tag{2}$$

In Equation (2), PET is potential evapotranspiration (mm/day), Δ is the slope of the vapor pressure curve (kPa·˚C^{-1}), R_n is net radiation at the surface (MJ·m^{-2}·day^{-1}), G is soil heat flux density (MJ·m^{-2}·day^{-1}, assumed = 0), γ is the psychrometric constant (kPa·˚C^{-1}), T is mean air temperature (˚C), U_2 is wind speed at 2 m height (m·s^{-1}), e_s is saturation vapor pressure (kPa), and e_a is actual vapor pressure (kPa) replaced by RH.

This method is preferably used since it takes into account both energy balance and aerodynamic factors, making it suitable to be used across diverse climatic zones to provide reliable results. The PET was further decomposed into contributions from its driving meteorological variables in order to assess their regional and seasonal influence on drying trends.

Linear trends in AI, precipitation, and PET were calculated using Ordinary Least Squares (OLS) at each grid cell, and statistical significance was assessed at $p < 0.05$. In this method, we did not apply adjustment for serial autocorrelation (e.g., pre-whitening or Modified Mann-Kendall) since the analysis focused on estimating the magnitude and spatial pattern of long-term trends at continental scale rather than testing individual grid-cell significance. This approach follows previous studies that utilized a similar approach (Abeysinghe et al., 2025; Chang et al.,

2024). Regional trends were derived from the aggregated time series, with 5-year running means applied to visualize decadal variability. PET changes were further decomposed into partial contributions of its primary drivers, namely T, RH, U, and available energy (AE), which is the difference between surface net radiation and soil heat flux density. This decomposition approach was adopted from Liu et al. (2024), where we treated the contributions of each variable separately to assess its influence on PET change while holding other variable constant. The methodology assumes interaction between meteorological variables are negligible and the total change in PET is the sum of these individual effects. The physical decomposition of the change in PET is expressed as follows: $\Delta PET = \Delta T + \Delta AE + \Delta RH + \Delta U$, while for aridity index $\Delta AI = \Delta P + \Delta PET$.

3. Results

3.1. Baseline Climatology and Aridity Patterns

The spatial distribution of aridity across Africa from 1951 to 2020 (Figure 1(a))

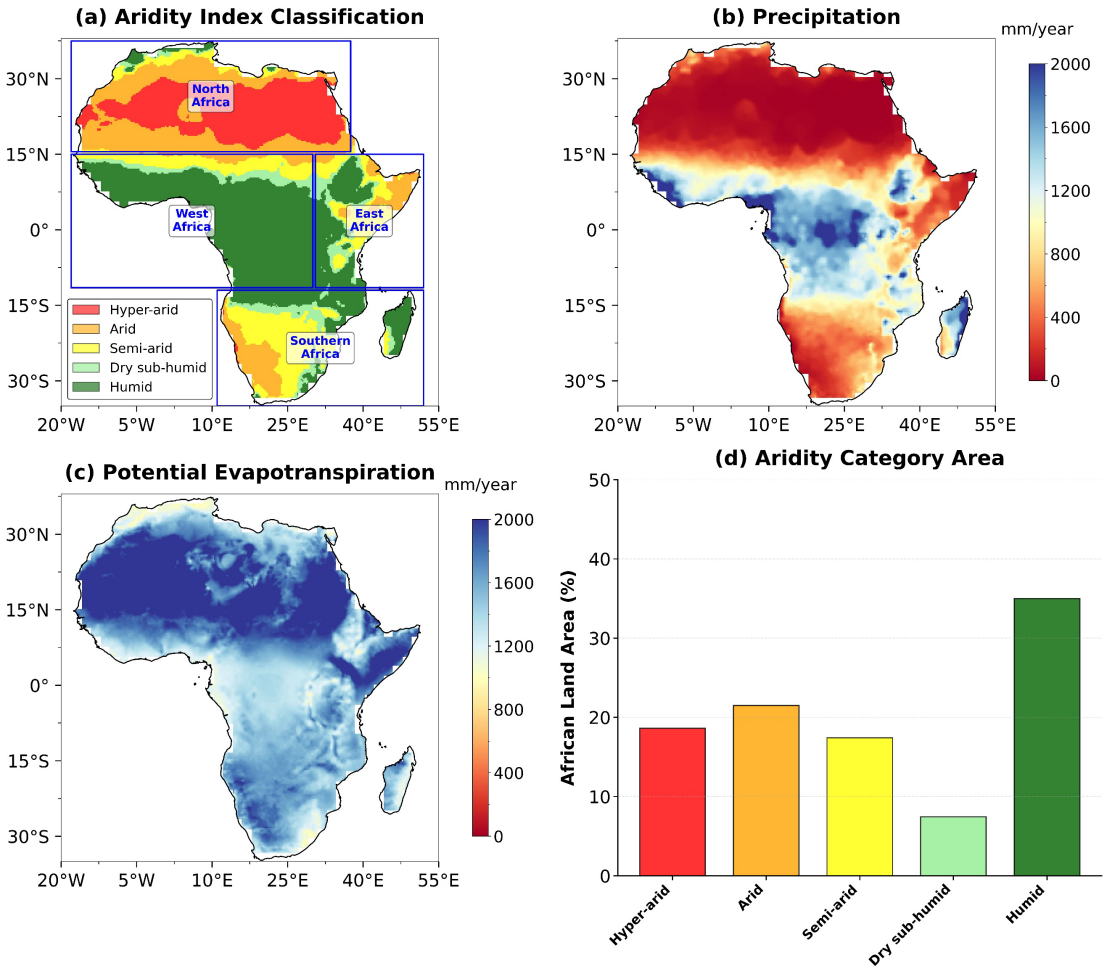

Figure 1. African Aridity Baseline (1951-2020). Spatial patterns of mean aridity and its key drivers: (a) Aridity classification based on the UNEP scheme using the mean annual Aridity Index. (b) Mean annual rainfall (mm/year). (c) Mean annual potential evapotranspiration (mm/year). (d) Area coverage (%) of each aridity class.

shows the mean annual state of AI, with classification based on the UNEP scheme. This provides a baseline for this study, highlighting long-term patterns of aridity and regional variations. Similarly, Figure 1(b), Figure 1(c) present mean annual precipitation and potential evapotranspiration (PET), highlighting distinct moisture availability and its variations across regions in Africa, while the extent of each aridity class and areal coverage is quantified in percentages (Figure 1(d)). In North Africa, which is classified as a hyper-arid region, minimal mean annual precipitation (~89 mm) is received, and the highest PET (~1902 mm/year) on the continent is experienced. Conversely, West Africa is identified as a humid region, where high rainfall reaches ~1261 mm/year and moderate PET (~1595 mm/year) is experienced. This gives a representation of how aridity is distributed across Africa to identify areas likely vulnerable to aridification.

3.2. Trends: Aridity, Precipitation, and Potential Evapotranspiration

The widespread drying conditions indicated by negative annual AI trends (Figure 2(a)) are prominent across large parts of Africa, covering about 88.9% of the total continent area, with 43% showing statistically significant drying, especially over the West African region. The mean decline in AI over the continent is −0.0012 yr^{-1}, corresponding to an 8.4% reduction over a 70-year period. Across all seasons, there is a consistent drying pattern, but the exception is SON, which registered the strongest mean trend of −0.0014 yr^{-1}, representing 29.1% significant area drying (Figure 2(m)). This significant drying pattern experienced over the seasons predominantly covers West Africa and part of East Africa across the seasons. The PET annual trend dominates Africa with 85.7% significant trends, while precipitation accounts for only 20.3% (Figure 2(b) and Figure 2(c)). This indicates the dominance of the PET-driven AI trend rather than precipitation in most places. On a seasonal scale, PET significant trends are 67.8% - 82.3%, while precipitation only covers 8.7% to 14.6% of the African continent (Figure 2). This suggests that PET spatially overshadows precipitation influence.

All four regions display universal drying trends but at varying intensities (Figures 3(a)-(t)). West Africa stands out, experiencing the most significant annual drying, with a trend of $\Delta AI = -0.0025\ yr^{-1}$ ($p < 0.01$; Figure 3(b)), and this pattern is persistent across all seasons. East Africa presents the next significant decreasing pattern during the annual and three of the seasons (JJA, MAM, and DJF). The annual trend here is $\Delta AI = -0.0011\ yr^{-1}$ ($p = 0.004$; Figure 3(c)). Southern Africa depicts a different pattern from East Africa, with a lower annual drying trend of $\Delta AI = -0.0009\ yr^{-1}$ ($p = 0.015$; Figure 3(d)). The season with the most significant seasonal drying trend for the region is SON (Figure 3(t)). However, North Africa exhibits the lowest annual AI drying trend compared to the three other regions (Figure 3(a)).

Overall, the analysis reveals the highest decreasing trend over western Africa, followed by East Africa, as compared to other regions.

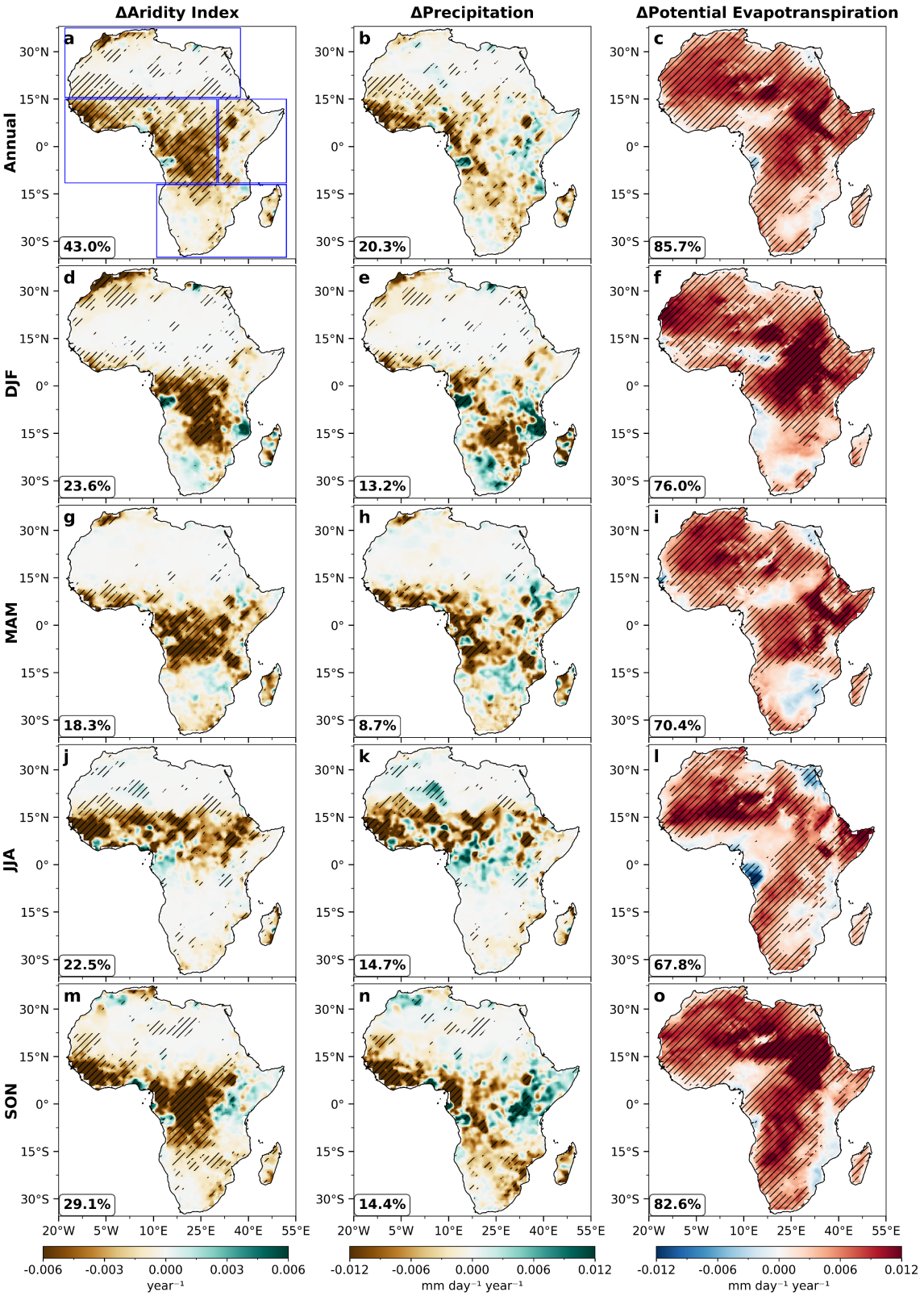

Figure 2. Seasonal trends (1951-2020) Aridity index (left column), Precipitation (middle), and potential evapotranspiration (right) across Africa. Rows show Annual, DJF, MAM, JJA, and SON. Hatching denotes changes significant at the 95% confidence level, indicated by percentage values (bottom-left).

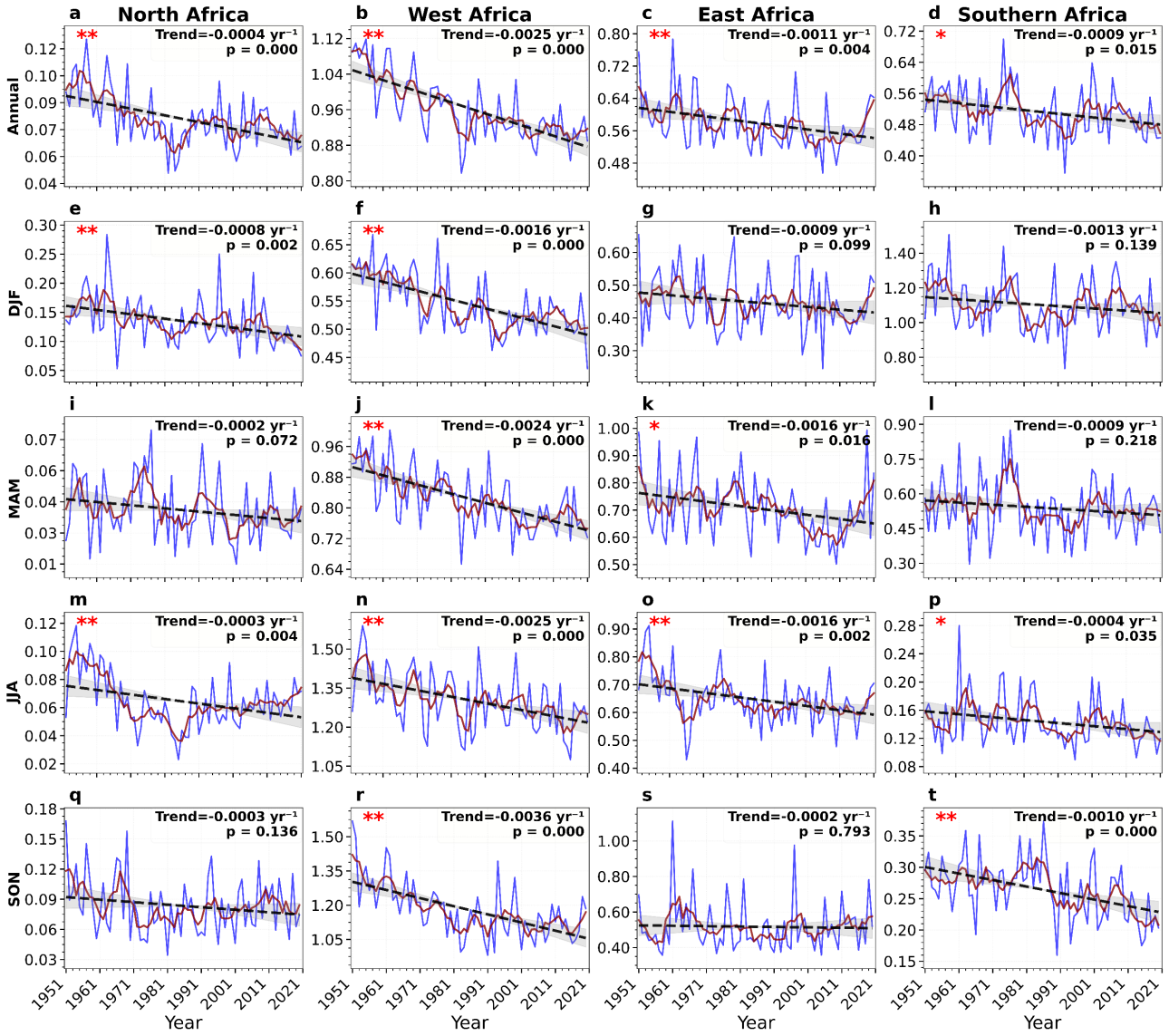

Figure 3. Regional Aridity Index (AI) trends across Africa (1951-2020) from (a) to (t) show time series of annual AI values (blue), linear trends (black dashed), 5-year running means (dark red), and 95% confidence intervals around the trend (gray shading). Each panel includes an annotation of the annual trend magnitude (yr^{-1}), percentage change per year, and the corresponding p-value. Statistical significance is indicated by asterisks in each panel, where * denotes $p < 0.05$, and ** denotes $p < 0.01$.

3.3. Attribution of AI Changes to Climate Drivers

We further analysed ΔP and ΔPET to evaluate their influence on aridity across the continent, as shown in **Figure 4**. Spatially, PET emerges as the most coherent driver of African aridification during 1951-2020, covering a wide area during annual and all seasonal periods, representing 86.1%-98.5% of Africa (**Figure 4**). This widespread increase in the PET signal aligns closely with the increase in temperature, explaining about 82.1%-98.4% of the rising atmospheric moisture demand. However, precipitation changes exhibit an uneven distribution pattern, revealing greater spatial heterogeneity. Here, precipitation only explains 20.3% of the drying signals annually, whereas individual seasons register 8.7%-14.6%.

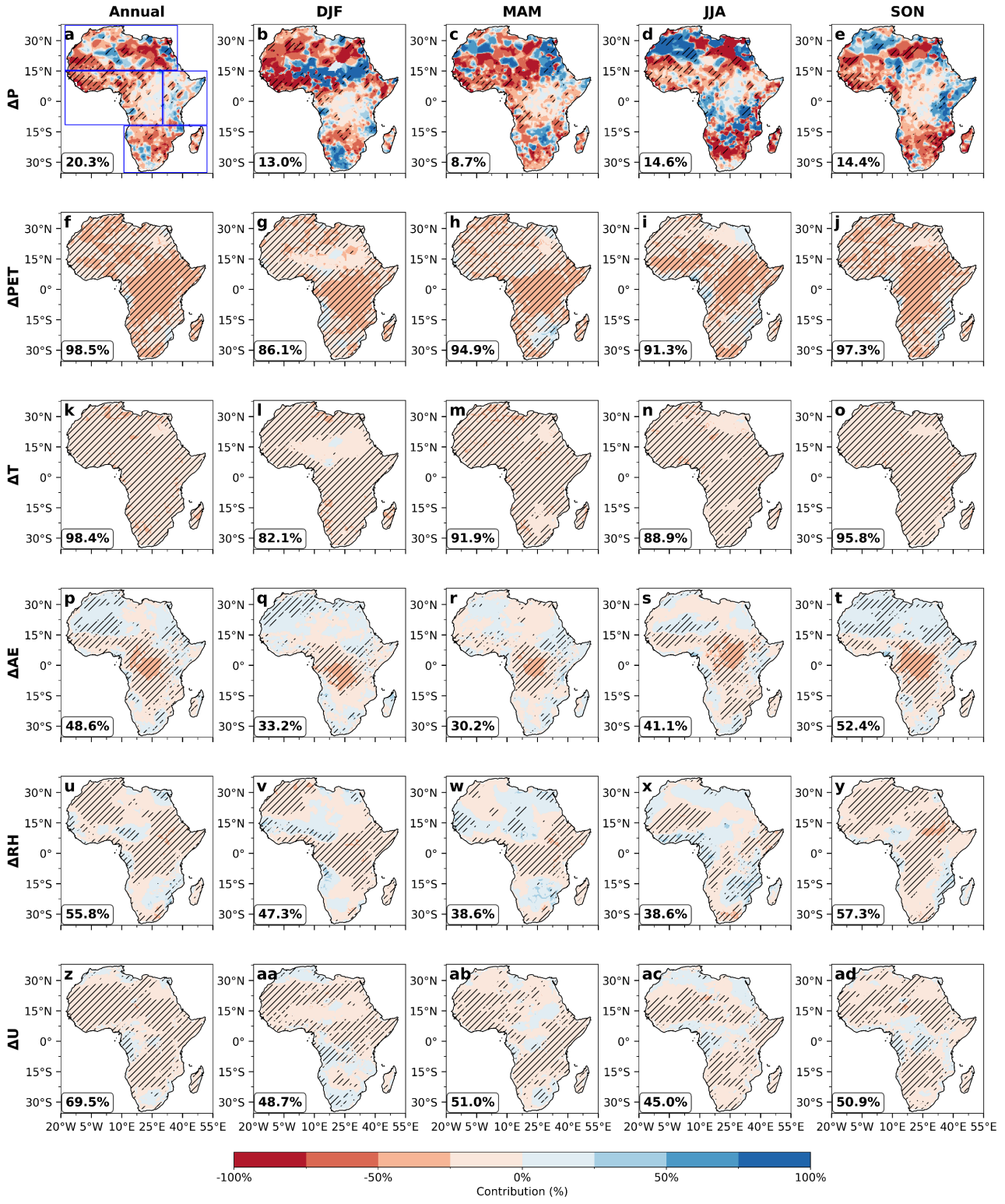

Figure 4. Contributions to AI changes (1951-2020) from precipitation change (ΔP), potential evapotranspiration change (ΔPET), temperature change (ΔT), available energy change (ΔAE), relative humidity change (ΔRH), and wind speed change (ΔU). The columns show annual and seasonal arrangements from left to right (Annual, DJF, MAM, JJA, SON). Hatching and percentages (bottom-left) indicate grid cells with statistically significant contributions ($p < 0.05$). Physical decomposition follows: $\Delta PET = \Delta T + \Delta AE + \Delta RH + \Delta U$, $\Delta AI = \Delta P + \Delta PET$.

We extended the analysis to examine the relative contributions of precipitation and PET at the regional level. The results vary across the four study regions (Figure 5), where over West Africa, annual aridification is induced by increasing PET, followed closely by declining precipitation (Figure 5(b)). In this region, the PET increase is consistent with reduced available energy and rising temperature,

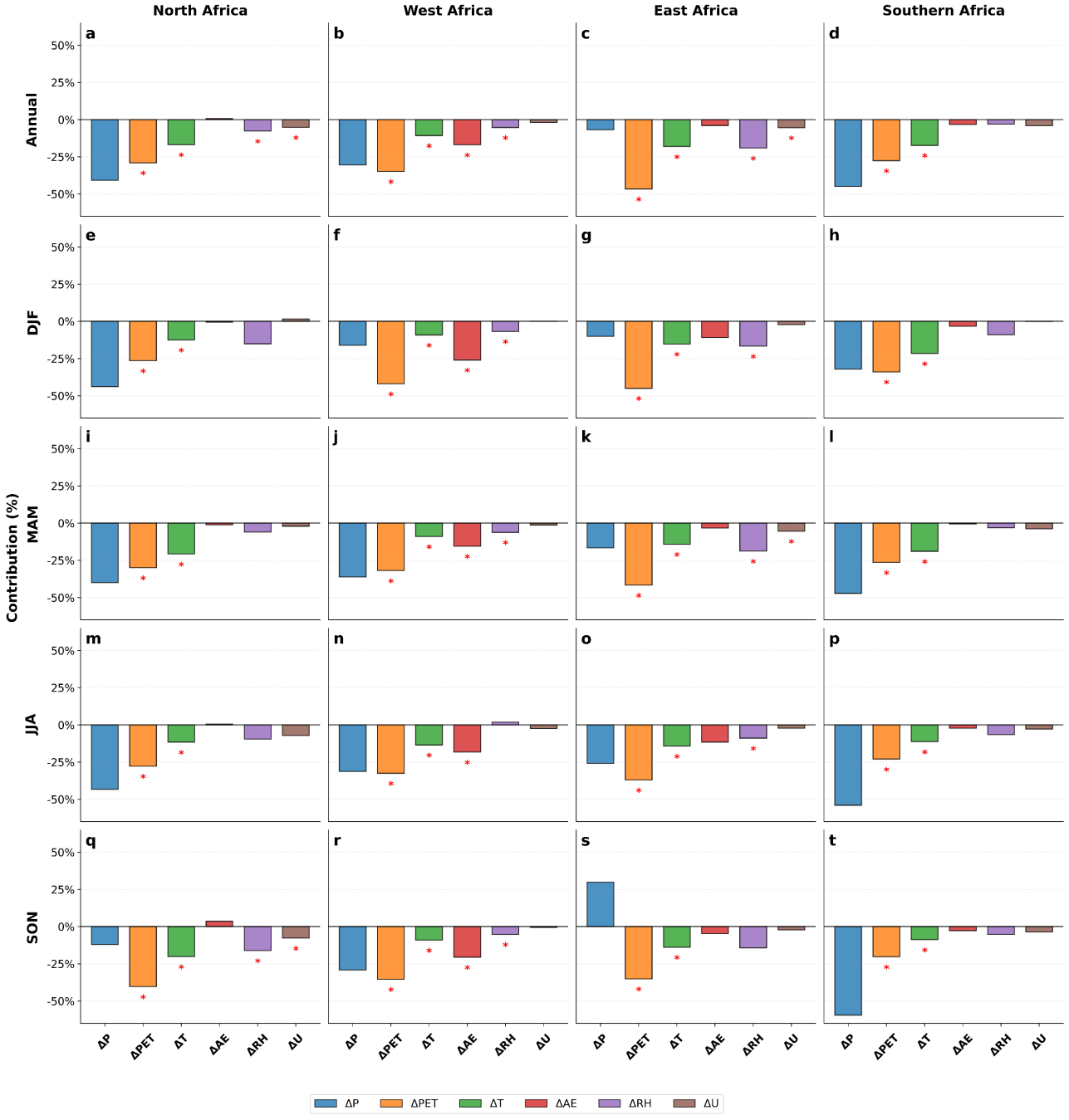

Figure 5. Regional mean contributions of climate drivers to Aridity Index (AI) trends (1951-2020). Rows: seasons (Annual, DJF, MAM, JJA, SON); columns: regions. Bars show average contribution percentages: ΔP (blue), ΔPET (orange), ΔT (green), ΔAE (red), ΔRH (purple), ΔU (brown). Negative values: drying contributions; positive values: moistening. Red asterisks (*) indicate sub-regional contributions where ≥50% of the grid cells are statistically significant ($p < 0.05$).

suggesting a warming environment driving increased atmospheric moisture demand. Here, the influence of RH and wind speed is very minimal, suggesting a strong influence of thermodynamic factors, unlike aerodynamic factors driving rising PET; however, precipitation change remains an important factor in the region.

Similarly, East Africa drying patterns indicate the influence of PET across all seasons, explaining close to one-half of the overall drying. Unlike West Africa, this drying arises from the combined effects of rising temperature and declining relative humidity. The situation is different during the SON season, where precipitation plays a moderating role on the effect of the strong PET contribution, partially proving moistening, resulting in minimizing net drying only to −4.9%.

In Southern Africa, the results are different as precipitation deficits here control much of the annual drying in the region. The strongest drying effect from precipitation decline is observed during SON, with PET contributing less than half of it (**Figure 5(t)**). This dominance is similarly visible during other seasons. PET increases contribute to additional drying, but their influence is considerably weaker compared to declining precipitation. Precipitation dominance in driving aridification over Southern Africa is consistent across all seasons. DJF shows elevated atmospheric demand, marked by rising temperature overshadowing the precipitation effect in regulating aridification.

Over North Africa, annual aridification is strongly driven by precipitation deficits, compared with −28.9% from ΔPET (**Figure 5(a)**). This mechanism is similar to that in Southern Africa. However, during the SON season, increases in PET exceed the precipitation effect on aridity, reflecting the growing role of PET (**Figure 5(q)**). This seasonal dominance of PET was observed to be driven by a rise in temperature and a decline in humidity in the region.

Overall, these results reveal that aridification in different regions of Africa has its own mechanisms. West and East Africa are influenced by rising PET, highlighting their sensitivity to warming and atmospheric drying, whereas Southern Africa is dominated by precipitation deficits, reflecting its vulnerability to rainfall change. Similar dependence on precipitation is also observed in North Africa, with a seasonal shift in aridification contribution from precipitation-dominated to PET-driven drying in SON. Therefore, based on these patterns, there is a need for adaptation strategies at the regional level, addressing both declining water availability and rising atmospheric moisture demand.

3.4. Transitions in Aridity Categories

Analysis of the shift in aridity categories between the early (1951-1984) and late (1985-2020) periods across Africa (**Figure 6**) reveals a highly heterogeneous pattern defined by regional and seasonal distinctions. We reveal that Southern Africa emerges as a hotspot for widespread aridity intensification, shifting from semi-arid to arid conditions, while dry sub-humid regions degrade towards semi-arid conditions (**Figure 6(e)**). The hyper-arid Namib Desert is also expanding, highlighting aridification across the region. Despite these aridification patterns being

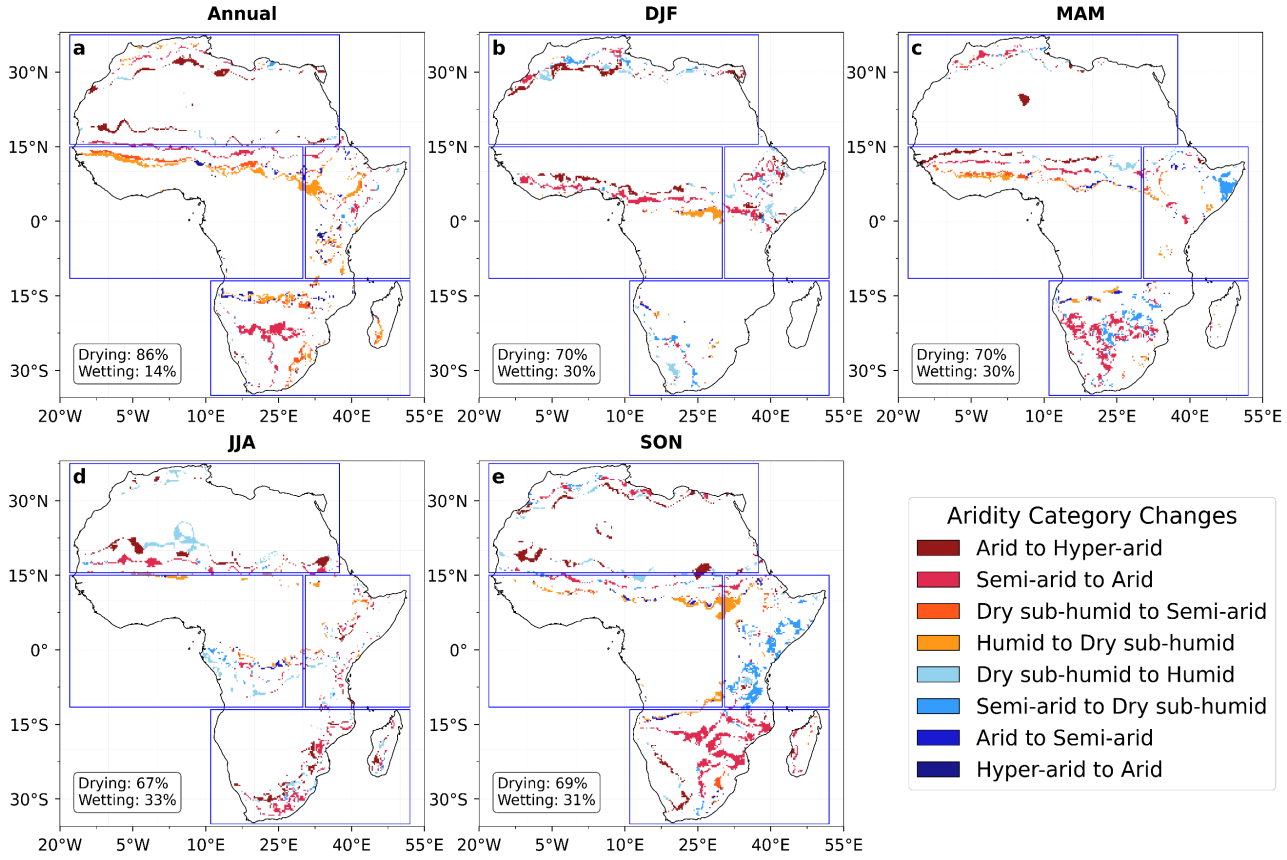

Figure 6. Seasonal aridity category transitions across Africa between 1951-1984 and 1985-2020. Panels show (a) Annual and seasonal (b) to (c) for DJF, MAM, JJA, and SON) shifts among five aridity classes (Hyper-arid to Humid). Colors indicate drying (red to orange) and wetting (blues) transitions of varying severity.

visible across other seasons, DJF showed a contrasting signal of seasonal recovery as the rainy season begins over Southern Africa (**Figure 6(b)**). This demonstrates the critical role of the inter-seasonal cycle in modulating the drying shifts in the regions.

Similar complexity is observed in East Africa, where seasonal divergence challenges a narrative of uniform aridification. Despite the annual signal showing a net shift toward drier conditions (**Figure 6(a)**), the SON season exhibits a widespread moistening pattern, characterized by a transition from the semi-arid to dry sub-humid category during the later period (**Figure 6(e)**). Another similar moistening signal was also detected in East Africa but was confined to the Horn of Africa during MAM (**Figure 6(c)**).

In West Africa, drying pattern transitions were observed from predominantly humid to dry sub-humid, while semi-arid conditions shifted to arid conditions, reaching their peak during the dry DJF season, signifying the expansion of the region toward more arid conditions. However, the rainy JJA season presents seasonal relief from aridification in the region (**Figure 6(d)**).

North Africa, mainly characterized by the hyper-arid Sahara Desert, maintains its persistent climatic conditions. The results here reveal a dominant transition

category within the arid spectrum from arid to hyper-arid, signaling an intensification and spatial expansion of existing extreme dryness. We identified minimal seasonal modulation to aridification in the region due to the rainy JJA season shifting northwards, causing hyper-arid regions to become arid (**Figure 6(d)**).

4. Summary and Discussion

This study provides robust potential evidence of aridification across Africa during 1951-2020. Our findings reveal an AI decline in approximately 43% of Africa at a 95% confidence level, indicating a broad intensification of dry conditions. The findings consistently coincide with regional and global assessments of aridity. In previous studies, widespread expansion in dryland across subtropical and semi-arid regions was reported (Greve et al., 2019; Sardans et al., 2024).

This suggests that arid conditions are spreading across Africa, making aridification a dominant hydroclimatic signal on the continent.

Furthermore, our finding reveals that increases in PET emerge as the main driver of observed aridification over Africa rather than precipitation alone. The results further demonstrate that the statistically significant trend in PET dominates over 86.1% of the continent, while precipitation does not exceed 20.3% of the total area. Moreover, the decomposition of PET indicates that temperature appears to be the main contributing factor controlling PET, accounting for more than 82.1% of the spatial variability, suggesting that warming across the continent is more likely linked to the temperature-PET relationship, consistent with global studies that suggest an increase in decoupling between rainfall variability and land surface moisture conditions (Greve et al., 2019; Huang, Yu, et al., 2016; Sardans et al., 2024). In addition, the dominance of PET in driving AI trends was linked to greenhouse warming, while precipitation exhibits a weaker response in AI trends reduction over the tropics and subtropics regions (Scheff & Frierson, 2015).

PET dominates both annually and across all seasons. In East Africa, we observed a decline in AI trends during SON and MAM despite an increase in seasonal rainfall trends. This demonstrates that short-term rainfall gains are overwhelmed by warming-driven atmospheric demand, insufficient to reverse the effect of high evaporative losses resulting in net drying conditions. Recent studies support this interpretation; for example, Ayugi et al. (2025) also found out that temperature variation plays a major role in influencing aridity over East Africa. In their findings, 82.2% of aridity variations are influenced by temperature, while precipitation only accounts for 40.2%. Their results also reported persistent arid conditions even during wet years, implying that long-term aridity in the region is not only influenced by precipitation variability. Similarly, Lim Kam Sian et al. (2024) study reported warming trend observed across Africa, which closely aligns with PET increase in East Africa together with higher precipitation in the latest climate normals (1991-2020). These further support findings of the growing influence of warming on hydroclimatic conditions in the region. Similar observations were made in West Africa, where more rainfall occurring during the JJA

monsoon season does not override the drying effect in the region, implying that the role of the atmospheric demand effect induced by rising temperature has more influence on regional aridification. In this case, the results demonstrate that short-term wet events or seasonal rainfall rarely offset the drying long-term aridification effect occurring due to rising atmospheric moisture demand (Huang, Yu, et al., 2016; Sardans et al., 2024).

Across regions in Africa, there are discrepancies in the drying trend and their associated drivers, even though the continent shows an overall decline in AI. Southern Africa exhibits a declining trend in AI, consistent with a decline in precipitation, while feedbacks from PET increase are secondary, particularly in the SON season. Southern Africa emerged as a hotspot of precipitation decline-induced aridification, which is closely related to the occurrence of ENSO conditions where El Niño phases led to droughts in the region (Greve et al., 2019; Sardans et al., 2024). Intensification of droughts was also linked to precipitation declines, accounting for about 25.6% during 1960-2007 (Sardans et al., 2024). Other studies also observed dryness in Southern Africa and listed long-term circulation shifts as a major factor amplifying dryness in the region (Chivangulula et al., 2025; Huang et al., 2016). North Africa remains hyper-arid, consistent with results; observations indicate that arid regions are becoming hyper-arid, implying an expansion of aridification. In this region, the annual drying trend appears to be driven by precipitation declines; however, for the SON season, the relative contribution from relative humidity reduction and warming emerges as a factor enhancing PET, thereby overshadowing the effects of precipitation. Since in hyper-arid regions like the Sahara, rainfall is so little, even a minimal increase in atmospheric moisture demand potentially leads to substantial dryness (Crapart et al., 2025; Huang et al., 2016). There is agreement in the results, both associating hyper-arid areas to their sensitive nature to changes in PET mainly induced by warming (Greve et al., 2019). North Africa is characterized as a hotspot for climate change, mostly associated with high risk of drought, high temperature, and limited adaptation capacity (Schilling et al., 2020).

We further investigate whether aridity categories have shifted over the years. The results indicated that West, East, and Southern Africa underwent some category shift, not just variability in aridity conditions. Since 1985, observations indicate that humid and dry sub-humid areas have likely shifted towards the semi-arid category, while previously semi-arid areas have become more arid in these areas associated with PET-driven drying. This implies that aridification induced by a rise in warming-driven atmospheric moisture demand might reshape climate systems, resulting from shifts in aridity categories, while the precipitation effect might be overshadowed (Asadi Zarch et al., 2017). However, the declining trend of precipitation appears to be the controlling factor of aridification in Southern Africa, where semi-arid areas are shifting into the arid class, signifying a different mechanism for dryness in the region compared to other regions (Huang et al., 2016). Africa is experiencing a transition towards drier classes, implying a long-

term persistent change rather than short-term variability. Similar patterns were also identified in other studies aligning with our study, amplifying evidence of the expansion of aridity in hyper-arid, arid, and semi-arid regions, associating these with climate warming (Asadi Zarch et al., 2017; Huang et al., 2016).

In summary, aridification observed over East, West, and North Africa indicates a potential water crisis even when seasonal rainfall can reduce the impact in these areas. We speculate worsening vulnerability to drought and reduced rainfall in Southern Africa due to the intensification of these arid conditions. We recommend strategies that consider growing atmospheric moisture demand in coping with the effects of aridification under global warming (Bedair et al., 2023; Sardans et al., 2024). Additionally, adaptation efforts should target individual regions to address water supply reduction and worsening impacts of increasing atmospheric evaporative demand alongside precipitation decline.

Acknowledgements

The first author sincerely acknowledges the Malawi Government, through the Department of Climate Change and Meteorological Services (DCCMS), for facilitating participation in the Master's Degree program. He also extends appreciation to Nanjing University of Information Science & Technology for academic guidance and to the Ministry of Commerce of the People's Republic of China (MOFCOM) for the scholarship enabling this study. Special thanks go to the supervisor, Professor Shanshan Liu, for valuable guidance and discussions throughout the research. Finally, the author acknowledges the use of GPCC precipitation and ERA5-Land reanalysis datasets, which were essential for the analyses presented in this study.

Conflicts of Interest

The authors declare no conflicts of interest regarding the publication of this paper.

References

Abate, S. G., Mekonnen, Y. G., Ambaye, B. A., Belay, A. M., Habtie, D. G., Tadesse, K. B. et al. (2025). Ecological Insights of Dryland Wetlands for Climate Resilience and Its Challenges in Sub-Saharan Africa. *Discover Environment, 3,* Article No. 175. https://doi.org/10.1007/s44274-025-00379-4

Abeysinghe, U., Balkissoon, S., & Aloysius, N. (2025). Assessment of Hydroclimatic Variability and Aridity Trends in the Mississippi River Basin Using Parametric and Non-Parametric Techniques. *Frontiers in Climate, 7,* Article ID: 1481926. https://doi.org/10.3389/fclim.2025.1481926

Akpa, A. F. (2024). The Effects of Climate Extreme Events on Selected Food Crop Yields in Sub-Saharan Africa. *Heliyon, 10,* e30796. https://doi.org/10.1016/j.heliyon.2024.e30796

Allen, R. G., Pereira, L. S., Raes, D., & Smith, M. (1998). *Crop Evapotranspiration: Guidelines for Computing Crop Water Requirements (FAO Irrigation and Drainage Paper No. 56).* Food and Agriculture Organization of the United Nations.

Asadi Zarch, M. A., Sivakumar, B., Malekinezhad, H., & Sharma, A. (2017). Future Aridity

under Conditions of Global Climate Change. *Journal of Hydrology, 554,* 451-469. https://doi.org/10.1016/j.jhydrol.2017.08.043

Ayugi, B. O., Oo, K. T., Umwali, E. D., & Alupot, D. (2025). Physical Predictand Drivers and Characteristics of Aridity across East Africa. *International Journal of Climatology,* e70212. https://doi.org/10.1002/joc.70212

Ayugi, B., Eresanya, E. O., Onyango, A. O., Ogou, F. K., Okoro, E. C., Okoye, C. O. et al. (2022). Review of Meteorological Drought in Africa: Historical Trends, Impacts, Mitigation Measures, and Prospects. *Pure and Applied Geophysics, 179,* 1365-1386. https://doi.org/10.1007/s00024-022-02988-z

Bedair, H., Alghariani, M. S., Omar, E., Anibaba, Q. A., Remon, M., Bornman, C. et al. (2023). Global Warming Status in the African Continent: Sources, Challenges, Policies, and Future Direction. *International Journal of Environmental Research, 17,* Article No. 45. https://doi.org/10.1007/s41742-023-00534-w

Cai, W., Reason, C., Mohino, E., Rodríguez-Fonseca, B., Malherbe, J., Santoso, A. et al. (2025). Climate Impacts of the El Niño-Southern Oscillation in Africa. *Nature Reviews Earth & Environment, 6,* 503-520. https://doi.org/10.1038/s43017-025-00705-7

Chang, M.-H., Huang, Y.-C., Cheng, Y.-H., Terng, C.-T., Chen, J., & Jan, J. C. (2024). Revisiting Regression Methods for Estimating Long-Term Trends in Sea Surface Temperature. *Natural Hazards and Earth System Sciences, 24,* 2481-2494. https://doi.org/10.5194/nhess-24-2481-2024

Chivangulula, F. M., Amraoui, M., & Pereira, M. G. (2025). The Drought Regime in Southern Africa and Recent Climate Change: Long-Term Trends in Climate Elements, Drought Indices and Descriptors. *Water, 17,* Article No. 3031. https://doi.org/10.3390/w17213031

Crapart, C., Anquetin, S., Blanchet, J., & Diedhiou, A. (2025). Global Projections of Aridity Index for Mid and Long-Term Future Based on CMIP6 Scenarios. *Hydrology and Earth System Sciences, 30,* 163-181. https://doi.org/10.5194/egusphere-2024-3710

Daramola, M. T., Eresanya, E. O., & Erhabor, S. C. (2023). How Has Aridity Changed over West Africa in the Past Four Decades? *Journal of African Earth Sciences, 197,* Article ID: 104745. https://doi.org/10.1016/j.jafrearsci.2022.104745

De Haan, C. (2016). *Prospects for Livestock-Based Livelihoods in Africa's Drylands*. World Bank. https://doi.org/10.1596/978-1-4648-0836-4

Dendoncker, M., Taugourdeau, S., Messier, C., & Vincke, C. (2023). A Functional Trait-Based Approach to Evaluate the Resilience of Key Ecosystem Functions of Tropical Savannas. *Forests, 14,* Article No. 291. https://doi.org/10.3390/f14020291

Dyer, E. L. E., Jones, D. B. A., Nusbaumer, J., Li, H., Collins, O., Vettoretti, G. et al. (2017). Congo Basin Precipitation: Assessing Seasonality, Regional Interactions, and Sources of Moisture. *Journal of Geophysical Research: Atmospheres, 122,* 6882-6898. https://doi.org/10.1002/2016jd026240

Feng, S., & Fu, Q. (2013). Expansion of Global Drylands under a Warming Climate. *Atmospheric Chemistry and Physics, 13,* 10081-10094. https://doi.org/10.5194/acp-13-10081-2013

Greve, P., Roderick, M. L., & Seneviratne, S. I. (2017). Simulated Changes in Aridity from the Last Glacial Maximum to 4xCO_2. *Environmental Research Letters, 12,* Article ID: 114021. https://doi.org/10.1088/1748-9326/aa89a3

Greve, P., Roderick, M. L., Ukkola, A. M., & Wada, Y. (2019). The Aridity Index under Global Warming. *Environmental Research Letters, 14,* Article ID: 124006. https://doi.org/10.1088/1748-9326/ab5046

Hassler, B., & Lauer, A. (2021). Comparison of Reanalysis and Observational Precipitation Datasets Including ERA5 and WFDE5. *Atmosphere, 12,* Article 1462. https://doi.org/10.3390/atmos12111462

Huang, J., Ji, M., Xie, Y., Wang, S., He, Y., & Ran, J. (2016). Global Semi-Arid Climate Change over Last 60 Years. *Climate Dynamics, 46,* 1131-1150. https://doi.org/10.1007/s00382-015-2636-8

Huang, J., Yu, H., Guan, X., Wang, G., & Guo, R. (2016). Accelerated Dryland Expansion under Climate Change. *Nature Climate Change, 6,* 166-171. https://doi.org/10.1038/nclimate2837

Iturbide, M., Gutiérrez, J. M., Alves, L. M., Bedia, J., Cerezo-Mota, R., Cimadevilla, E. et al. (2020). An Update of IPCC Climate Reference Regions for Subcontinental Analysis of Climate Model Data: Definition and Aggregated Datasets. *Earth System Science Data, 12,* 2959-2970. https://doi.org/10.5194/essd-12-2959-2020

Li, F., Diop, S., Hirwa, H., Maesho, S., Ning, X., Tian, C. et al. (2024). Dryland Social-Ecological Systems in Africa. In B. Fu, & M. Stafford-Smith (Eds.), *Dryland Social-Ecological Systems in Changing Environments* (pp. 273-323). Springer. https://doi.org/10.1007/978-981-99-9375-8_9

Lim Kam Sian, K. T. C., Sagero, P., & Ongoma, V. (2024). Precipitation, Temperature and Potential Evapotranspiration for 1991-2020 Climate Normals over Africa. *Theoretical and Applied Climatology, 155,* 5465-5482. https://doi.org/10.1007/s00704-024-04963-1

Liu, S., & Zhou, X. (2023). The PMIP4 Simulated Dryland Aridity Changes during the Last Interglacial. *Environmental Research Letters, 18,* Article ID: 094056. https://doi.org/10.1088/1748-9326/acf725

Liu, W., Zhang, B., Wei, Z., Wang, Y., Tong, L., Guo, J. et al. (2024). Heterogeneity Analysis of Main Driving Factors Affecting Potential Evapotranspiration Changes across Different Climate Regions. *Science of the Total Environment, 912,* Article ID: 168991. https://doi.org/10.1016/j.scitotenv.2023.168991

Masih, I., Maskey, S., Mussá, F. E. F., & Trambauer, P. (2014). A Review of Droughts on the African Continent: A Geospatial and Long-Term Perspective. *Hydrology and Earth System Sciences, 18,* 3635-3649. https://doi.org/10.5194/hess-18-3635-2014

Middleton, N. J., & Thomas, D. S. G. (1997). *World Atlas of Desertification*. Arnold.

Mohino, E., Monerie, P., Mignot, J., Diakhaté, M., Donat, M., Roberts, C. D. et al. (2024). Impact of Atlantic Multidecadal Variability on Rainfall Intensity Distribution and Timing of the West African Monsoon. *Earth System Dynamics, 15,* 15-40. https://doi.org/10.5194/esd-15-15-2024

Mortimore, M., & Anderson, S. (2009). *Dryland Opportunities: A New Paradigm for People, Ecosystems and Development*. IUCN; IIED; UNDP.

Muñoz-Sabater, J., Dutra, E., Agustí-Panareda, A., Albergel, C., Arduini, G., Balsamo, G., et al. (2021). ERA5-Land: A State-of-the-Art Global Reanalysis Dataset for Land Applications. *Earth System Science Data, 13,* 4349-4383. https://doi.org/10.5194/essd-13-4349-2021

Nicholson, S. E. (2013). The West African Sahel: A Review of Recent Studies on the Rainfall Regime and Its Interannual Variability. *ISRN Meteorology, 2013,* Article ID: 453521. https://doi.org/10.1155/2013/453521

Nicholson, S. E., Funk, C., & Fink, A. H. (2018). Rainfall over the African Continent from the 19th through the 21st Century. *Global and Planetary Change, 165,* 114-127. https://doi.org/10.1016/j.gloplacha.2017.12.014

Noël, T., Loukos, H., Defrance, D., Vrac, M., & Levavasseur, G. (2022). Extending the

Global High-Resolution Downscaled Projections Dataset to Include CMIP6 Projections at Increased Resolution Coherent with the ERA5-Land Reanalysis. *Data in Brief, 45,* Article ID: 108669. https://doi.org/10.1016/j.dib.2022.108669

Qiao, L., Zuo, Z., & Xiao, D. (2022). Evaluation of Soil Moisture in CMIP6 Simulations. *Journal of Climate, 35,* 779-800. https://doi.org/10.1175/jcli-d-20-0827.1

Sardans, J., Miralles, A., Tariq, A., Zeng, F., Wang, R., & Peñuelas, J. (2024). Growing Aridity Poses Threats to Global Land Surface. *Communications Earth & Environment, 5,* Article No. 776. https://doi.org/10.1038/s43247-024-01935-1

Scheff, J., & Frierson, D. M. W. (2015). Terrestrial Aridity and Its Response to Greenhouse Warming across CMIP5 Climate Models. *Journal of Climate, 28,* 5583-5600. https://doi.org/10.1175/jcli-d-14-00480.1

Schilling, J., Hertig, E., Tramblay, Y., & Scheffran, J. (2020). Climate Change Vulnerability, Water Resources and Social Implications in North Africa. *Regional Environmental Change, 20,* 1-12. https://doi.org/10.1007/s10113-020-01597-7

Schneider, U., Hänsel, S., Finger, P., Rustemeier, E., & Ziese, M. (2022). *GPCC Full Data Monthly Version 2022 at 0.25°: Monthly Land-Surface Precipitation from Rain-Gauges Built on GTS-Based and Historic Data: Globally Gridded Monthly Totals (Version 2022, p. min. 20 MB-max. 300 MB per Gzip Archive (10 Years per Archive)) [NetCDF].* Global Precipitation Climatology Centre (GPCC) at Deutscher Wetter-Dienst. https://doi.org/10.5676/DWD_GPCC/FD_M_V2022_025

Ullah, S., You, Q., Sachindra, D. A., Nowosad, M., Ullah, W., Bhatti, A. S. et al. (2022). Spatiotemporal Changes in Global Aridity in Terms of Multiple Aridity Indices: An Assessment Based on the CRU Data. *Atmospheric Research, 268,* Article ID: 105998. https://doi.org/10.1016/j.atmosres.2021.105998

Wei, F., Wang, S., Brandt, M., Fu, B., Meadows, M. E., Wang, L. et al. (2021). Responses and Feedbacks of African Dryland Ecosystems to Environmental Changes. *Current Opinion in Environmental Sustainability, 48,* 29-35. https://doi.org/10.1016/j.cosust.2020.09.004

Yessoufou, A. N., Kumar, S., Houessionon, P., Worou, O. N., Wane, A., & Whitbread, A. (2024). Vulnerability and Resilience in the Face of Climate Changes in Senegal's Drylands: Measurement at the Household Level and Determinant Assessment. *Frontiers in Climate, 6,* Article ID: 1330025. https://doi.org/10.3389/fclim.2024.1330025